The Astrophysical Journal Letters, 717:L127–L132, 2010 July 10 doi:10.1088/2041-8205/717/2/L127

FERMI OBSERVATIONS OF HIGH-ENERGY GAMMA-RAY EMISSION FROM GRB 090217A

M. Ackermann[1], M. Ajello[1], L. Baldini[2], J. Ballet[3], G. Barbiellini[4,5], M. G. Baring[6], D. Bastieri[7,8], K. Bechtol[1], R. Bellazzini[2], B. Berenji[1], P. N. Bhat[9], E. Bissaldi[10], R. D. Blandford[1], E. Bonamente[11,12], A. W. Borgland[1], A. Bouvier[1], J. Bregeon[2], A. Brez[2], M. S. Briggs[9], M. Brigida[13,14], P. Bruel[15], R. Buehler[1], S. Buson[7,8], G. A. Caliandro[16], R. A. Cameron[1], P. A. Caraveo[17], S. Carrigan[8], J. M. Casandjian[3], C. Cecchi[11,12], Ö. Çelik[18,19,20], E. Charles[1], A. Chekhtman[21,22], J. Chiang[1], S. Ciprini[12], R. Claus[1], J. Cohen-Tanugi[23], V. Connaughton[9], J. Conrad[24,25,65], S. Cutini[26], C. D. Dermer[21], A. de Angelis[27], F. de Palma[13,14], S. W. Digel[1], E. do Couto e Silva[1], P. S. Drell[1], R. Dubois[1], C. Favuzzi[13,14], S. J. Fegan[15], E. C. Ferrara[18], M. Frailis[27,28], Y. Fukazawa[29], P. Fusco[13,14], F. Gargano[14], D. Gasparrini[26], N. Gehrels[18], S. Germani[11,12], N. Giglietto[13,14], P. Giommi[26], F. Giordano[13,14], M. Giroletti[30], T. Glanzman[1], G. Godfrey[1], J. Granot[31], I. A. Grenier[3], J. E. Grove[21], L. Guillemot[32,33,34], S. Guiriec[9], D. Hadasch[35], E. Hays[18], D. Horan[15], R. E. Hughes[36], G. Jóhannesson[1], A. S. Johnson[1], W. N. Johnson[21], T. Kamae[1], H. Katagiri[29], R. M. Kippen[37], J. Knödlseder[38], D. Kocevski[1], M. Kuss[2], J. Lande[1], L. Latronico[2], S.-H. Lee[1], M. Llena Garde[24,25], F. Longo[4,5], F. Loparco[13,14], M. N. Lovellette[21], P. Lubrano[11,12], A. Makeev[21,22], M. N. Mazziotta[14], S. McBreen[10,39], J. E. McEnery[18,40], S. McGlynn[41,25], C. Meegan[42], J. Mehault[23], P. Mészáros[43], P. F. Michelson[1], T. Mizuno[29], A. A. Moiseev[19,40], C. Monte[13,14], M. E. Monzani[1], E. Moretti[4,5], A. Morselli[44], I. V. Moskalenko[1], S. Murgia[1], H. Nakajima[45], T. Nakamori[46], M. Naumann-Godo[3], P. L. Nolan[1], J. P. Norris[47], E. Nuss[23], M. Ohno[48], T. Ohsugi[49], A. Okumura[48], N. Omodei[1], E. Orlando[10], J. F. Ormes[47], M. Ozaki[48], W. S. Paciesas[9], D. Paneque[1], J. H. Panetta[1], D. Parent[21,22], V. Pelassa[23], M. Pepe[11,12], M. Pesce-Rollins[2], V. Petrosian[1], F. Piron[23], T. A. Porter[1], R. Preece[9], J. L. Racusin[18], S. Rainò[13,14], R. Rando[7,8], A. Rau[10], M. Razzano[2], S. Razzaque[21,50], A. Reimer[51,1], O. Reimer[51,1], J. Ripken[24,25], M. Roth[52], F. Ryde[25,41], H. F.-W. Sadrozinski[53], A. Sander[36], J. D. Scargle[54], T. L. Schalk[53], C. Sgrò[2], E. J. Siskind[55], P. D. Smith[36], G. Spandre[2], P. Spinelli[13,14], M. Stamatikos[18,36], M. S. Strickman[21], D. J. Suson[56], H. Tajima[1], H. Takahashi[49], T. Tanaka[1], J. B. Thayer[1], J. G. Thayer[1], L. Tibaldo[7,8,3,66], D. F. Torres[16,35], G. Tosti[11,12], A. Tramacere[1,57,58], T. Uehara[29], T. L. Usher[1], J. Vandenbroucke[1], A. J. van der Horst[59,67], V. Vasileiou[19,20], N. Vilchez[38], V. Vitale[44,60], A. von Kienlin[10], A. P. Waite[1], P. Wang[1], C. Wilson-Hodge[59], B. L. Winer[36], K. S. Wood[21], X. F. Wu[43,61,62], R. Yamazaki[63], Z. Yang[24,25], T. Ylinen[41,64,25], and M. Ziegler[53]

[1] W. W. Hansen Experimental Physics Laboratory, Kavli Institute for Particle Astrophysics and Cosmology, Department of Physics and SLAC National Accelerator Laboratory, Stanford University, Stanford, CA 94305, USA
[2] Istituto Nazionale di Fisica Nucleare, Sezione di Pisa, I-56127 Pisa, Italy
[3] Laboratoire AIM, CEA-IRFU/CNRS/Université Paris Diderot, Service d'Astrophysique, CEA Saclay, 91191 Gif sur Yvette, France
[4] Istituto Nazionale di Fisica Nucleare, Sezione di Trieste, I-34127 Trieste, Italy
[5] Dipartimento di Fisica, Università di Trieste, I-34127 Trieste, Italy
[6] Department of Physics and Astronomy, Rice University, MS-108, P.O. Box 1892, Houston, TX 77251, USA
[7] Istituto Nazionale di Fisica Nucleare, Sezione di Padova, I-35131 Padova, Italy
[8] Dipartimento di Fisica "G. Galilei," Università di Padova, I-35131 Padova, Italy
[9] Center for Space Plasma and Aeronomic Research (CSPAR), University of Alabama in Huntsville, Huntsville, AL 35899, USA
[10] Max-Planck Institut für extraterrestrische Physik, 85748 Garching, Germany; azk@mpe.mpg.de
[11] Istituto Nazionale di Fisica Nucleare, Sezione di Perugia, I-06123 Perugia, Italy
[12] Dipartimento di Fisica, Università degli Studi di Perugia, I-06123 Perugia, Italy
[13] Dipartimento di Fisica "M. Merlin" dell'Università e del Politecnico di Bari, I-70126 Bari, Italy
[14] Istituto Nazionale di Fisica Nucleare, Sezione di Bari, 70126 Bari, Italy
[15] Laboratoire Leprince-Ringuet, École polytechnique, CNRS/IN2P3, Palaiseau, France
[16] Institut de Ciencies de l'Espai (IEEC-CSIC), Campus UAB, 08193 Barcelona, Spain
[17] INAF-Istituto di Astrofisica Spaziale e Fisica Cosmica, I-20133 Milano, Italy
[18] NASA Goddard Space Flight Center, Greenbelt, MD 20771, USA
[19] Center for Research and Exploration in Space Science and Technology (CRESST) and NASA Goddard Space Flight Center, Greenbelt, MD 20771, USA
[20] Department of Physics and Center for Space Sciences and Technology, University of Maryland Baltimore County, Baltimore, MD 21250, USA
[21] Space Science Division, Naval Research Laboratory, Washington, DC 20375, USA
[22] George Mason University, Fairfax, VA 22030, USA
[23] Laboratoire de Physique Théorique et Astroparticules, Université Montpellier 2, CNRS/IN2P3, Montpellier, France; piron@lpta.in2p3.fr
[24] Department of Physics, Stockholm University, AlbaNova, SE-106 91 Stockholm, Sweden
[25] The Oskar Klein Centre for Cosmoparticle Physics, AlbaNova, SE-106 91 Stockholm, Sweden
[26] Agenzia Spaziale Italiana (ASI) Science Data Center, I-00044 Frascati (Roma), Italy; sarac@slac.stanford.edu
[27] Dipartimento di Fisica, Università di Udine and Istituto Nazionale di Fisica Nucleare, Sezione di Trieste, Gruppo Collegato di Udine, I-33100 Udine, Italy
[28] Osservatorio Astronomico di Trieste, Istituto Nazionale di Astrofisica, I-34143 Trieste, Italy
[29] Department of Physical Sciences, Hiroshima University, Higashi-Hiroshima, Hiroshima 739-8526, Japan
[30] INAF Istituto di Radioastronomia, 40129 Bologna, Italy
[31] Centre for Astrophysics Research, Science and Technology Research Institute, University of Hertfordshire, Hatfield AL10 9AB, UK
[32] Max-Planck-Institut für Radioastronomie, Auf dem Hügel 69, 53121 Bonn, Germany
[33] CNRS/IN2P3, Centre d'Études Nucléaires Bordeaux Gradignan, UMR 5797, Gradignan 33175, France
[34] Université de Bordeaux, Centre d'Études Nucléaires Bordeaux Gradignan, UMR 5797, Gradignan 33175, France
[35] Institució Catalana de Recerca i Estudis Avançats (ICREA), Barcelona, Spain
[36] Department of Physics, Center for Cosmology and Astro-Particle Physics, The Ohio State University, Columbus, OH 43210, USA
[37] Los Alamos National Laboratory, Los Alamos, NM 87545, USA
[38] Centre d'Étude Spatiale des Rayonnements, CNRS/UPS, BP 44346, F-30128 Toulouse Cedex 4, France

[39] University College Dublin, Belfield, Dublin 4, Ireland
[40] Department of Physics and Department of Astronomy, University of Maryland, College Park, MD 20742, USA
[41] Department of Physics, Royal Institute of Technology (KTH), AlbaNova, SE-106 91 Stockholm, Sweden
[42] Universities Space Research Association (USRA), Columbia, MD 21044, USA
[43] Department of Astronomy and Astrophysics, Pennsylvania State University, University Park, PA 16802, USA
[44] Istituto Nazionale di Fisica Nucleare, Sezione di Roma "Tor Vergata," I-00133 Roma, Italy
[45] Department of Physics, Tokyo Institute of Technology, Meguro City, Tokyo 152-8551, Japan
[46] Research Institute for Science and Engineering, Waseda University, 3-4-1, Okubo, Shinjuku, Tokyo 169-8555, Japan
[47] Department of Physics and Astronomy, University of Denver, Denver, CO 80208, USA
[48] Institute of Space and Astronautical Science, JAXA, 3-1-1 Yoshinodai, Sagamihara, Kanagawa 229-8510, Japan
[49] Hiroshima Astrophysical Science Center, Hiroshima University, Higashi-Hiroshima, Hiroshima 739-8526, Japan
[50] National Research Council Research Associate, National Academy of Sciences, Washington, DC 20001, USA
[51] Institut für Astro- und Teilchenphysik and Institut für Theoretische Physik, Leopold-Franzens-Universität Innsbruck, A-6020 Innsbruck, Austria
[52] Department of Physics, University of Washington, Seattle, WA 98195-1560, USA
[53] Department of Physics and Department of Astronomy and Astrophysics, Santa Cruz Institute for Particle Physics, University of California at Santa Cruz, Santa Cruz, CA 95064, USA
[54] Space Sciences Division, NASA Ames Research Center, Moffett Field, CA 94035-1000, USA
[55] NYCB Real-Time Computing Inc., Lattingtown, NY 11560-1025, USA
[56] Department of Chemistry and Physics, Purdue University Calumet, Hammond, IN 46323-2094, USA
[57] Consorzio Interuniversitario per la Fisica Spaziale (CIFS), I-10133 Torino, Italy
[58] INTEGRAL Science Data Centre, CH-1290 Versoix, Switzerland
[59] NASA Marshall Space Flight Center, Huntsville, AL 35812, USA
[60] Dipartimento di Fisica, Università di Roma "Tor Vergata," I-00133 Roma, Italy
[61] Joint Center for Particle Nuclear Physics and Cosmology (J-CPNPC), Nanjing 210093, China
[62] Purple Mountain Observatory, Chinese Academy of Sciences, Nanjing 210008, China
[63] Aoyama Gakuin University, Sagamihara-shi, Kanagawa 229-8558, Japan
[64] School of Pure and Applied Natural Sciences, University of Kalmar, SE-391 82 Kalmar, Sweden
Received 2010 May 6; accepted 2010 June 8; published 2010 June 22

ABSTRACT

The *Fermi* observatory is advancing our knowledge of gamma-ray bursts (GRBs) through pioneering observations at high energies, covering more than seven decades in energy with the two on-board detectors, the Large Area Telescope (LAT) and the Gamma-ray Burst Monitor (GBM). Here, we report on the observation of the long GRB 090217A which triggered the GBM and has been detected by the LAT with a significance greater than 9σ. We present the GBM and LAT observations and on-ground analyses, including the time-resolved spectra and the study of the temporal profile from 8 keV up to ∼1 GeV. All spectra are well reproduced by a Band model. We compare these observations to the first two LAT-detected, long bursts GRB 080825C and GRB 080916C. These bursts were found to have time-dependent spectra and exhibited a delayed onset of the high-energy emission, which are not observed in the case of GRB 090217A. We discuss some theoretical implications for the high-energy emission of GRBs.

Key words: gamma-ray burst: individual (GRB090217A)

1. INTRODUCTION

Gamma-ray bursts (GRBs) are the most extreme events in the universe and have fascinated astronomers since their discovery 40 years ago (Klebesadel et al. 1973). Until 2008, only a small fraction of GRBs had been detected at energies above the MeV region (Hurley et al. 1994; Gonzalez et al. 2003; Giuliani et al. 2008). The *Fermi Gamma-ray Space Telescope* was launched on 2008 June 11, and it provides unprecedented energy coverage and sensitivity for the study of high-energy emission in GRBs. It is composed of two instruments: the Gamma-ray Burst Monitor (GBM; Meegan et al. 2009) and the Large Area Telescope (LAT; Atwood et al. 2009). The GBM monitors the entire unocculted sky. It covers four decades in energy through the combination of 12 NaI and 2 BGO scintillation detectors, which are sensitive in the energy ranges 8 keV to 1 MeV and 150 keV to 40 MeV, respectively. The LAT is a pair conversion telescope which consists of 4×4 arrays of silicon strip trackers and cesium iodide calorimeter modules covered by a segmented anti-coincidence detector designed to efficiently reject charged particle background events. The energy coverage of the LAT instrument ranges from 20 MeV to more than 300 GeV, with a field of view of ∼2.4 sr at 1 GeV.

After 18 months of operations, the LAT instrument has detected 15 GRBs at energies above 100 MeV, including two short bursts.[68] After GRB 080825C (Abdo et al. 2009b) and GRB 080916C (Abdo et al. 2009a), GRB 090217A is the third long burst which was firmly detected with the LAT above 100 MeV after triggering the GBM. Section 2 addresses the detection and localization of this burst and presents the light curves from both instruments. The joint spectral analysis is described in Section 3. In Section 4, the results are discussed in the context of other LAT-detected long GRBs and current theoretical models, and our conclusions are given in Section 5.

2. GBM AND LAT OBSERVATIONS

2.1. GBM Observations

At 04:56:42.56 UTC on 2009 February 17 (T_0), the *Fermi* GBM triggered and located GRB 090217A (trigger 256539404/090217206; von Kienlin 2009). This bright, long GRB was

[65] Royal Swedish Academy of Sciences Research Fellow, funded by a grant from the K. A. Wallenberg Foundation.
[66] Partially supported by the International Doctorate on Astroparticle Physics (IDAPP) program.
[67] NASA Postdoctoral Program Fellow, USA.

[68] See the LAT GRB table: http://fermi.gsfc.nasa.gov/ssc/resources/observations/grbs/grb_table

detected by NaI detectors numbers 6–11 which are located on one side of the spacecraft. Four of these detectors exceeded the threshold and the GBM triggered on 256 ms timescale in the energy range 50–300 keV. The BGO detector located on the same side, B1, detected emission up to ∼1 MeV. In fact, the emission from GRB 090217A was so intense that it was detected through the spacecraft by most of the NaI detectors and indeed the BGO detector (B0) on the opposite side.

The angle of GRB 090217A to the LAT boresight was 35°, placing this bright, hard event firmly in the field of view. The GBM on-ground localization reported by von Kienlin (2009) was unusually far (∼9°) from the early LAT localization (Ohno et al. 2009). However, this was improved upon using a response table for spectrally hard, bright bursts (such as GRB 090217A) that also accounts for saturation events. The final GBM position is (R.A., decl.) = (205.°5, −6.°0) with a statistical error of ∼1° and a standard systematic uncertainty of 2°–3° (Briggs et al. 2009), and is consistent with the LAT position.

The light curves from the GBM and LAT are shown in Figure 1, sorted from top to bottom in order of increasing energy. The first two panels display the background-subtracted light curves for the NaI and the BGO detectors. The first panel shows the sum of the counts of the three NaI detectors (N6, N8, and N9) with the strongest signal in the 8–260 keV band. The second panel shows the corresponding plot for the sum of both BGO detector counts, between 260 keV and 5 MeV. GRB 090217A features a structured light curve in the GBM energy band, with one major peak with substructures and many overlapping pulses. The burst duration estimates for the 8 keV to 1 MeV range are $T_{90} = 32.8$ s and $T_{50} = 11.3$ s. The LAT light curves in the last three panels are described in Section 2.2.2.

2.2. LAT Observations

2.2.1. Detection and Localization

GRB 090217A did not trigger the LAT onboard detection algorithm and was found through a blind search in the LAT data by the on ground Automated Science Processing (ASP) pipeline (Band et al. 2009). Subsequently and independent of the ASP analysis, the detection was confirmed by searches of the GBM location. The first step of this study is selecting the LAT events belonging to the so-called TRANSIENT class (Atwood et al. 2009) of the "P6_V3" analysis.[69] This selection provides a large effective area with a reasonable background rate adapted for burst detection and localization.

The unbinned likelihood method for localization makes use of the LAT point-spread function (PSF) on an event-by-event basis. The instrument response functions (IRFs) have not been validated below 100 MeV, thus we restrict this analysis to being above this spectroscopic threshold. Following the methodology described in detail in Abdo et al. (2009b), we computed the LAT position of GRB 090217A using the map of the Test Statistics (TS), considering all TRANSIENT events recorded above 100 MeV between T_0 and $T_0 + 37.5$ s in a region of 15° centered on the final GBM position. GRB 090217A occurred at a relatively high Galactic latitude ($b \sim 53°$), thus the Galactic emission contributes only a few percent of the total background. Therefore, only an isotropic component, largely residual charged-particle events, was included in the background model.

To compute the detection significance and the localization error, the TS values are interpreted in terms of the χ^2 distribution with two degrees of freedom. The best fit position is found to be (R.A., decl.) = (204.°73, −8.°43), which is 0.°17 away from the early localization (Ohno et al. 2009), with a $TS_{max} = 89$ corresponding to a 9.2σ detection. The TS contours around this position yielded the 68%, 90%, and 99% statistical error radii, respectively of 0.°37, 0.°54, and 0.°80. As explained in (Abdo et al. 2009b), the relatively small inclination angle of GRB 090217A in the LAT field of view implies a negligible systematic error (< 0.°1).

We also searched for a temporally extended emission above 100 MeV, as observed in other LAT long bright bursts, e.g., GRB 080916C (Abdo et al. 2009a) and GRB 090902B (Abdo et al. 2009c). This unbinned likelihood analysis is based on the LAT events belonging to the so-called DIFFUSE class, which is suited to searches on longer time scales (Abdo et al. 2009b). GRB 090217A remained within 60° from the LAT boresight until $T_0 + 500$ s, but no additional signal was found by this time. Finally, despite Swift Target of Opportunity observations of the early LAT localization, no X-ray afterglow was found (Godet 2009) and hence there is no redshift available for this burst.

2.2.2. Count Light Curves from Energy-dependent Spatial Event Selections

Unlike the unbinned likelihood analysis, the joint GBM-LAT spectral study and the study of the burst temporal profile in the LAT do not make use of the LAT PSF on an event-by-event basis. In these analyses, an increased signal-to-background ratio is obtained for the LAT by selecting the events in a region of interest (ROI) centered on the final LAT position. As described in Abdo et al. (2009b), its size (r_{ROI}) is energy dependent and is obtained as the 95% containment radius of the LAT PSF added in quadrature to the LAT localization error.

We split the LAT TRANSIENT events into "FRONT" and "BACK" data sets, respectively, including the events which converted in the upper and lower parts of the tracker, thus with different PSF widths (Atwood et al. 2009). We used a maximum size $r_{ROI}^{max} = 10°$–$12°$ for these two conversion types, which makes the size of the ROI saturate between 100 MeV and 200 MeV in both cases. All events resulting from this selection process are shown in the last two panels of Figure 1. The events above 100 MeV will be used for the joint GBM-LAT spectral analysis in Section 3. They are displayed in the last panel along with their energies as a function of time. A 447 MeV event is detected at $\sim T_0$ while the LAT event with the highest energy (866 MeV) arrives at $T_0 + 14.8$ s. Additional events are recorded up to ∼30 s after the trigger time.

The study of the temporal profile of the LAT emission which is discussed in Section 4 requires good photon statistics. In the case of GRB 090217A, this can be achieved by including events recorded at lower energies, i.e., the 27 TRANSIENT events above 50 MeV which are displayed in the fourth panel of Figure 1. As in Abdo et al. (2009b), the expected number of background events is computed by a procedure developed by the LAT collaboration to quantitatively estimate levels of residual charged-particle backgrounds. This estimator was found to provide accurate values of the TRANSIENT background level above 50 MeV within a 10%–15% systematic uncertainty. The computation of the probability that the observed number of counts is due to a background fluctuation is performed in a frequentist way, with a semi-Bayesian treatment of the systematic uncertainty. The time history of the corresponding cumulative significance for the gamma-ray signal is shown in Figure 2.

[69] http://www-glast.slac.stanford.edu/software/IS/glast_lat_performance.htm

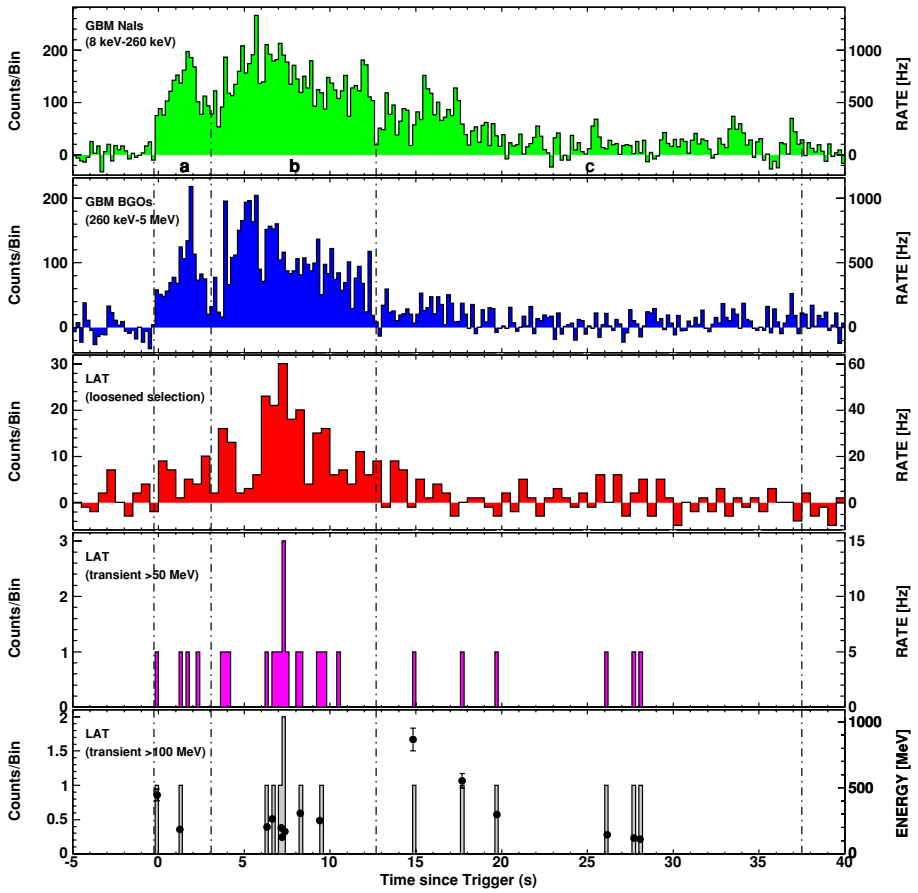

Figure 1. Light curves for GRB 090217A observed by the GBM and the LAT, from lowest to highest energies. The top three panels are background subtracted. The first panel shows the sum of the counts of the three NaI detectors (N6, N8, and N9) with the highest signal in the 8–260 keV band. The second panel shows the sum of both BGO detector counts, between 260 keV and 5 MeV. The LAT light curve shown in the third panel has been generated using events which passed the onboard gamma filter, with a direction compatible with the final LAT position (see the text). The binning is 0.5 s, while it is 0.2 s in the other panels. The last two panels have been generated from the LAT events which passed the TRANSIENT event selection above 50 MeV and 100 MeV, respectively. The events were selected within an ROI centered on the final LAT position, with a size decreasing with energy following the PSF energy dependence (see the text). Black dots, along with their error bars (uncertainty in the LAT energy measurement) represent the 1σ energy range (right y-axis) for each LAT event in the last panel. The vertical dash-dotted lines indicate the time bins used in the time-resolved spectral analysis.

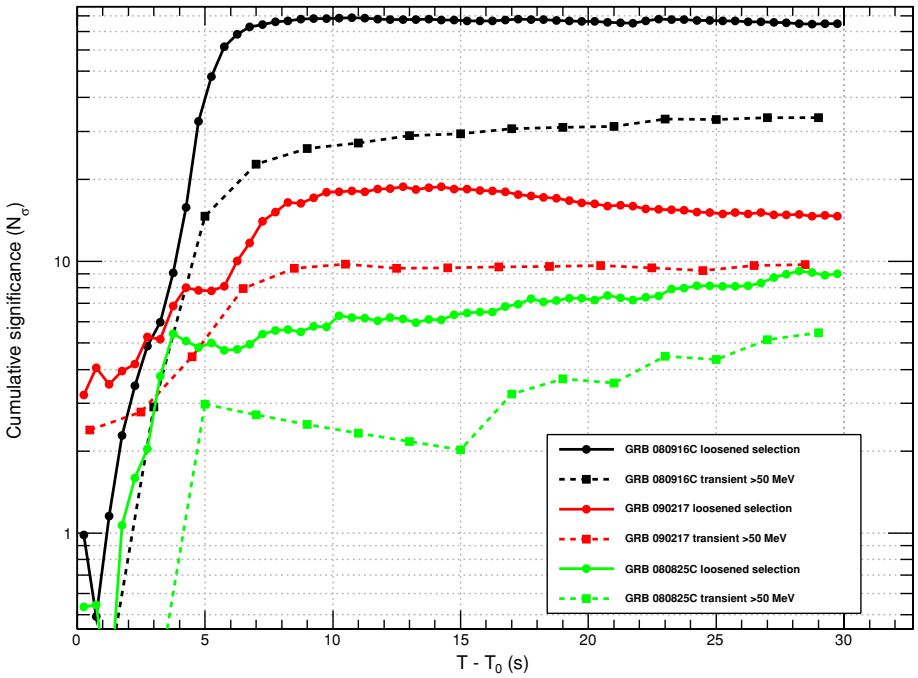

Figure 2. Time history of the cumulative significance of the LAT emission for GRB 090217A, using the loosened selection and the event selection above 50 MeV shown in the third and fourth panels in Figure 1. Similar curves for GRB 080825C and GRB 080916C are superimposed.

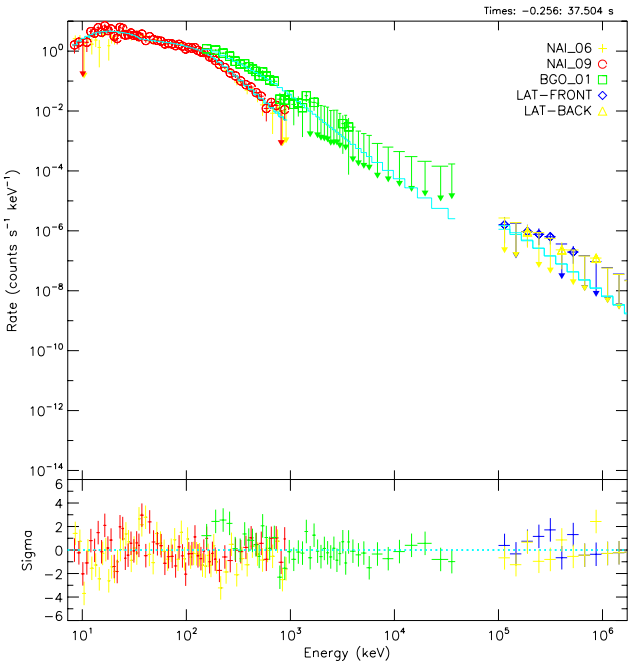

Figure 3. Time-averaged ($T_0 - 0.26$ s to $T_0 + 37.50$ s) count spectrum of GRB 090217A of the GBM (NaI and BGO) and LAT data. The spectrum is well fit by a Band function spanning five decades in energy. The LAT data have been separated into FRONT and BACK data sets (see the text).

As in Abdo et al. (2010), we also used a relaxed event selection, considering all LAT events that passed the onboard gamma filter. Most of these events have at least a well-reconstructed track in the tracker, thus providing a rough direction measurement. The corresponding PSF was found to be much worse than for the TRANSIENT class, with a 68% containment radius of ∼20°, ∼13°, and ∼7° at 20 MeV, 50 MeV, and 100 MeV, respectively. However, applying an additional spatial selection based on the 68% containment angles for this PSF reduced the background from ∼300 Hz to ∼16 Hz. The background-subtracted light curve obtained with this loosened event selection is shown in the third panel of Figure 1, and the time history of its cumulative significance is reported in Figure 2.

3. GBM AND LAT JOINT SPECTRAL ANALYSIS

Simultaneous spectral fits of the GBM and LAT data were performed for each of the three time bins (a–c) shown in Figure 1. The selected boundaries reflect the time characteristics of GBM features and LAT photons. The first time bin (a) starts 256 ms before the GBM trigger time in order to include the first LAT (447 MeV) event and lasts up to $T_0 + 3.072$ s. The central time bin (b) starts at $T_0 + 3.072$ s up to $T_0 + 12.672$ s, i.e., until the end of the main LAT emission. The last bin (c) starts at $T_0 + 12.672$ s and ends at $T_0 + 37.504$ s, covering the tail of the LAT and GBM emission. The 15 total events selected in the LAT are displayed in the last panel of Figure 1. As in Section 2.2.1, we used a spectroscopic threshold of 100 MeV to avoid any spurious result due to systematic uncertainties in the LAT IRFs. The spectral analysis was performed with the software package RMFIT (version 3.1), using binned GBM TTE data and selected LAT FRONT and BACK events (see details in Abdo et al. 2009b). Instead of a χ^2, we used the Castor C-statistic (Dorman et al. 2003) to simultaneously fit the combined data sets due to the small number of events at the highest energies. The Castor statistic

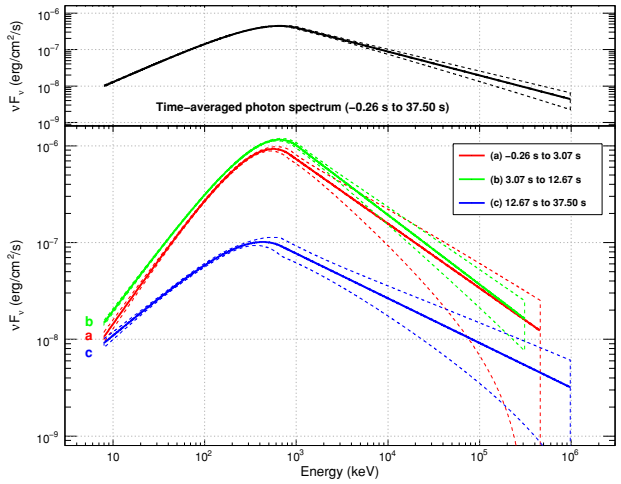

Figure 4. Spectral energy distributions for the Band models found in time bins (a)–(c) are shown in thick solid lines which reach the largest detected photon energy in each time bin, while the corresponding (same color) thin dashed lines represent the 68% confidence level contours for each fit.

is similar to the Cash statistic (Cash 1979), except for an offset that is constant for a particular data set.

All time-resolved count spectra are well fitted by a Band function, which consists of two smoothly connected power laws (Band et al. 1993). Figure 3 displays the time-averaged count spectrum, which spans five decades in energy and is also well reproduced by a Band model. The source photon spectral energy distributions are shown in Figure 4 with their 68% confidence level contours. The best fit model parameters are reported in Table 1 with their statistical errors along with the energy fluxes in the 20 keV–2 MeV and 100 MeV–10 GeV energy bands. The systematic errors on these parameters are essentially dominated by the uncertainty on the effective areas of the instruments. In Abdo et al. (2009b), we found a ±15% systematic uncertainty on the amplitude A, ±0.03 for the spectral slopes α and β, and ±8 keV for the peak energy $E_{\rm peak}$. For GRB 090217A, these uncertainties are negligible for β and $E_{\rm peak}$, while they are comparable to the statistical errors for α and dominant for A.

Whereas the time evolution of the amplitude and $E_{\rm peak}$ shows the same trend as the overall intensity of the burst, as observed from Figure 1, the low-energy slope (α) becomes gradually softer and the high-energy slope (β) remains constant within the quoted errors. In particular, the apparent hardening of β between time bins (b) and (c) is not significant ($\sim 1.5\sigma$). The hardness ratio between the low- and high-energy fluxes is also found to be constant, with a mean value of 0.026 ± 0.011 for the time-averaged spectrum.

4. COMPARISON TO THE LAT DETECTED GRB 080825C AND GRB 080916C

GRB 090217A does not exhibit any noticeable spectral feature, other than the common Band spectral shape, similar to the first two long bursts detected by the LAT, GRB 080825C, and GRB 080916C. In all three bursts, no significant excess in the form of an additional spectral component, or a deficit in the form of a spectral cutoff, was found in the LAT energy range with respect to the extrapolation of the Band spectrum from lower energies. In combination with correlated temporal behavior of the low and high energies, this suggests that a single emission mechanism accounts for the radiation across all energy bands. In Abdo et al. (2010), we estimated the fluence ratio of the 100 MeV–10 GeV energy band to the 20 keV–2 MeV energy

Table 1
Time-resolved and Time-averaged Spectral Analysis Results for GRB 090217A

	Time Range (s)	A	$E_{\rm peak}$	α	β	Energy Flux	
						GBM	LAT
(a)	−0.26–3.07	$21.4^{+1.2}_{-1.1}$	$562.5^{+57.4}_{-48.2}$	$-0.63^{+0.06}_{-0.06}$	$-2.67^{+0.13}_{-0.21}$	216.1 ± 8.9	4.9 ± 5.0
(b)	3.07–12.67	$23.7^{+0.6}_{-0.6}$	$652.7^{+35.5}_{-32.8}$	$-0.73^{+0.03}_{-0.03}$	$-2.72^{+0.08}_{-0.11}$	267.6 ± 5.8	5.0 ± 2.7
(c)	12.67–37.50	$4.4^{+0.5}_{-0.4}$	$430.5^{+125.0}_{-92.7}$	$-1.20^{+0.08}_{-0.06}$	$-2.46^{+0.10}_{-0.16}$	30.2 ± 2.3	1.7 ± 1.4
All	−0.26–37.50	$10.5^{+0.3}_{-0.3}$	$656.4^{+43.7}_{-39.4}$	$-0.89^{+0.03}_{-0.03}$	$-2.65^{+0.07}_{-0.08}$	108.8 ± 2.6	2.8 ± 1.2

Notes. Band function best fit parameters are provided for all spectra. The amplitude A of the Band function is given in units of 10^{-3} γ cm^{-2} s^{-1} keV^{-1}, its peak energy $E_{\rm peak}$ in keV. Energy fluxes are given in 10^{-8} erg cm^{-2} s^{-1}, in the energy ranges from 20 keV to 2 MeV for the GBM and from 100 MeV to 10 GeV for the LAT.

band to be ∼7% for GRB 080825C and ∼30% for GRB 080916C. The ratio of ∼3% found for GRB 090217A places this burst in a similar range as GRB 080825C.

Beyond these obvious similarities, GRB 090217A does not share several of the high-energy properties observed in the other two bursts. First of all, the onset of the high-energy emission of GRB 090217A is not much delayed with respect to the ∼100 keV radiation, and a continuous increase of the high-energy flux is observed at early times, as shown in Figures 1 and 2. Figure 2 also shows the time history of the cumulative significance for GRB 080916C and GRB 080825C. In spite of its brightness, GRB 080916C is not detected within the first ∼2 s, and then exhibits a very sharp rise between 3 s and 5 s. Given the poor photon statistics from the TRANSIENT event selection, we could not confirm the presence of a lag in the case of GRB 080825C (with a 3.4% chance probability), and simply noted that the first events recorded by the LAT from this burst were coincident with the second GBM peak (Abdo et al. 2009b). The light curve obtained with a loosened event selection confirms the absence of any excess at early times with a higher significance. GRB 080825C is significantly detected ($>5\sigma$) only after ∼4 s, with the bulk of its emission slowly accumulating up to 9σ within the next ∼25 s. GRB 090217A has a smoother evolution and the delayed onset of its emission in the LAT energy band is much less marked. It is marginally seen from the first instants and significantly detected after only ∼3 s. It reaches its maximum between 10 s and 15 s and does not last longer than the low-energy emission. This is the opposite to what was observed for the other two bursts: GRB 080916C showed evidence for a long-lasting LAT emission up to 1.4 ks, while GRB 080825C emission lasted somewhat longer in the LAT (up to T_0+35 s) than in the GBM (with a $T_{90} = 27$ s), with the highest energy photon arriving when the GBM emission was very weak. In Abdo et al. (2009b), we discussed the latter result as a possible detection of a separate and harder component showing up at late times. Finally, no strong spectral evolution was observed in GRB 090217A especially at the highest energies, unlike GRB 080916C which underwent a strong soft–hard–soft evolution.

5. DISCUSSION AND CONCLUSIONS

While other long LAT-detected bursts such as GRB 080825C and GRB 080916C exhibit a high-energy spectral variability associated with a delayed onset of the LAT emission along with a temporally extended emission, GRB 090217A is a firmly LAT-detected burst with featureless high-energy properties. The similarity of the temporal history of its gamma-ray emission over five decades in energy and the agreement, within the observational errors, between measured spectra with the Band model suggest that a single mechanism is responsible for the observed broadband emission.

As in the case of GRB 080916C, a simple leptonic mechanism appears to be the most straightforward choice to reproduce the observed emission, e.g., synchrotron emission or jitter radiation (Medvedev 2000). The low-energy spectral slope of all three time bins is compatible with a synchrotron mechanism (Preece et al. 1998), and the mild soft to hard to soft variation of $E_{\rm peak}$ could be due to episodes of different shell collisions leading to shocks with different parameters. More complicated scenarios are possible but not required by the present observations. Observations of more, and brighter, GRBs with both GBM and LAT in the near future will certainly help to assess what fraction of high-energy emitting bursts share similar properties, and to clarify the dominant emission mechanisms as well as the particle acceleration and cooling processes occurring in GRB jets.

The *Fermi* LAT Collaboration acknowledges support from a number of agencies and institutes for both development and the operation of the LAT as well as scientific data analysis. These include NASA and DOE in the United States, CEA/Irfu and IN2P3/CNRS in France, ASI and INFN in Italy, MEXT, KEK, and JAXA in Japan, and the K. A. Wallenberg Foundation, the Swedish Research Council, and the National Space Board in Sweden. Additional support from INAF in Italy and CNES in France for science analysis during the operations phase is also gratefully acknowledged. The *Fermi* GBM Collaboration acknowledges support for GBM development, operations and data analysis from NASA in the US and BMWi/DLR in Germany.

REFERENCES

Abdo, A. A., et al. 2009a, Science, 323, 1688
Abdo, A. A., et al. 2009b, ApJ, 707, 580
Abdo, A. A., et al. 2009c, ApJ, 706, L138
Abdo, A. A., et al. 2010, ApJ, 712, 558
Atwood, W. B., et al. 2009, ApJ, 697, 1071
Band, D., et al. 1993, ApJ, 413, 281
Band, D., et al. 2009, ApJ, 701, 1673
Briggs, M. S., et al. 2009, in Proc. AIP Conf. Ser. 1133, Gamma-ray Bursts: Sixth Huntsville Symp., ed. C. Meegan, N. Gehrels, & C. Kouveliotou (Melville, NY: AIP), 40
Cash, W. 1979, ApJ, 228, 939
Dorman, B., Arnaud, K. A., & Gordon, C. A. 2003, BAAS, 35, 641
Giuliani, A., et al. 2008, A&A, 491, L25
Godet, O. 2009, GCN, 8907, 1
Gonzalez, M. M., et al. 2003, Nature, 424, 749
Hurley, K., et al. 1994, Nature, 372, 652
Klebesadel, R. W., Strong, I. B., & Olson, R. A. 1973, ApJ, 182, L85
Medvedev, M. V. 2000, ApJ, 540, 704
Meegan, C., et al. 2009, ApJ, 702, 791
Ohno, M., et al. 2009, GCN, 8903, 1
Preece, R. D., et al. 1998, ApJ, 506, L23
von Kienlin, A. 2009, GCN, 8902, 1